IMPULSE PHOTOTHERMAL EVALUATION OF MATERIALS VIA FREQUENCY MODULATED OPTICAL REFLECTANCE II: EXPERIMENTAL

J.F. Power and A. Mandelis

Photoacoustic and Photothermal Sciences Laboratory
Department of Mechanical Engineering
University of Toronto
5 King's College Road
Toronto, Ontario
M5S 1A4 Canada

INTRODUCTION

Recently, a powerful method of photothermal detection was reported which enabled thermal wave imaging to be carried out on micron sized structures in semiconductors [1,2]. The new method utilized the photothermally induced modulation of the sample's surface optical reflectivity to detect thermal wave phenomena at bandwidths exceeding 10 MHz. The wide bandwidth capabilities of the method enabled very shallow structures to be analyzed in semiconducting materials because of the relationship that exists between the modulation frequency of the excitation beam and the thermal diffusion length.

In more recent work [3], transient changes in surface reflectivity were induced in the sample and followed by means of pulsed laser excitation. This second approach carries the advantage of a time visualization of the thermal response from buried subsurface layers, and enables the recording of a high resolution depth profile of the sample within a single excitation wavetrain. Some important disadvantages of pulsed excitation, however, are the associated high peak power of the impulse, (which may induce optical damage to the material under test), the high dynamic range requirements of the detection apparatus, non-idealities in the temporal pulse shape, large variations in the shot-to-shot energy and the overall inferior quality of the transverse mode structure associated with many pulsed (especially single pass) laser sources.

As an alternative to the use of pulsed laser sources in photothermal wave excitation, a powerful wideband excitation method which avoided the high peak power and associated disadvantages of the conventional pulsed techniques was recently introduced [4]. The new method, termed FM Time Delay Spectrometry, through its past applications in acoustics [5], generated photothermal wave phenomena in materials using low power linear frequency sweeps whose power spectra were flat within the modulation bandwidth of the sweep. This permitted the recovery of band limited impulse response information from the photothermal system under study.

In this work, we have extended the technique of FM Time Delay Spectrometry to the detection of impulse photothermoreflectance in solid state materials. We have assembled a fast photothermoreflectance

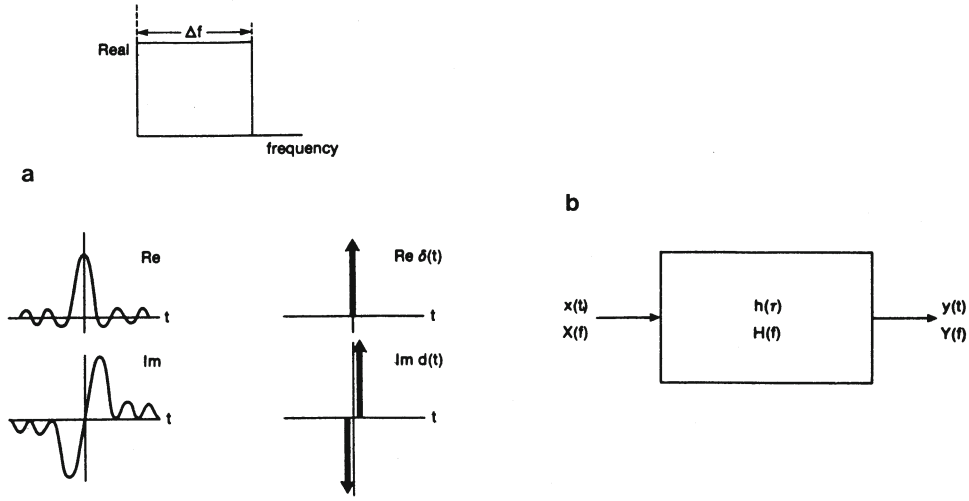

Fig. 1 (a) Schematic representation of a photothermal system as a generalized linear time-invariant system; (b) Frequency and time-delay domain representations of flatband frequency spectrum.

impulse response imager and evaluated its performance with some well characterized materials. We also demonstrate the uses of the wideband technique in thermal diffusivity measurements, and examine the conditions under which quantitative information may be obtained.

WIDEBAND EXCITATION AND FM TIME DELAY SPECTROMETRY

The general strategy of wideband methods in general is the excitation of a linear time invariant system with a wavetrain whose power spectrum is flat within the response bandwidth of the system. If one were to inverse Fourier transform the power spectral density function of the input wavetrain, the corresponding input autocorrelation function would be a good approximation to the Dirac delta function within the band limit set by the response of the system under study (Fig. 1).

Signal recovery in wideband excitation methods is typically achieved through correlation and spectral analysis. The acquisition and calculation of the required spectral density functions is conveniently achieved by means of the Weiner-Khinchin relations [6] in which successive Fourier transforms of the input and output wavetrains are computed and averaged. The corresponding cross and autocorrelation functions are computed by inverse Fourier transformation of the spectral density functions. The recovery of the linear system's impulse and frequency response information is then achieved by the following relations:

$$\text{In the time delay domain: } R_{xy}(\tau) = \int_0^{\tau} R_{xx}(t)\, h(t+\tau)\, dt \tag{1a}$$

$$\text{In the frequency domain: } G_{xy}(f) = \frac{H(f)}{G_{xx}(f)} \tag{1b}$$

The specific advance offered by FM Time Delay Spectrometry is the use of a linear frequency sweep for wideband excitation. Such waveforms possess good autospectral flatness and narrow autocorrelation halfwidth under conditions of sufficiently slow sweep times and sufficiently high frequency resolution. Because these waveforms are deterministic as opposed to purely stationary, FM time delay responses may

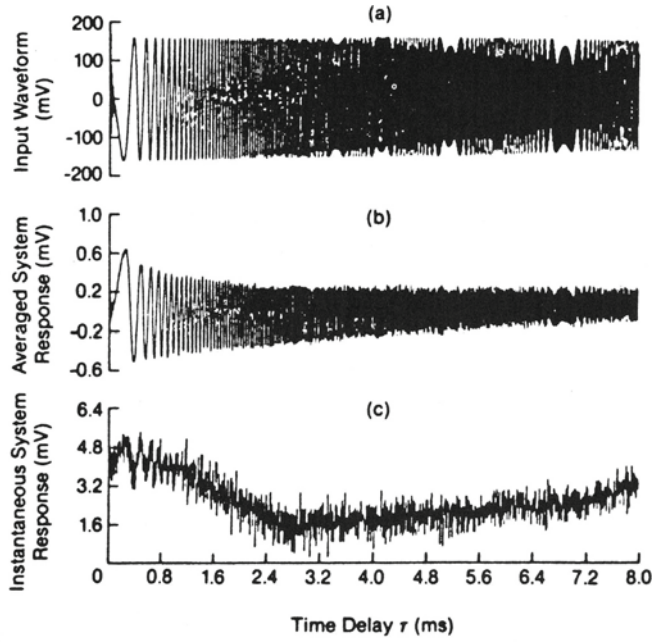

Fig. 2 Linear FM sweep wavetrains for photothermal response of semi-infinite sample of quartz. Sweep/measurement bandwidth: 0 to 100 kHz. Sweep rate: $S = 10^7$ Hz/s. (a) single excitation sweep; (b) time averaged photothermal response, N = 1,000 replicates; (c) single response time record.

be synchronously time averaged to improve signal to noise ratios. Also, the input autospectrum is essentially flat within a single sweep: unlike random noise excitation it is unnecessary to average many replicates of these waveforms in order to achieve autospectral flatness. Some examples of the photothermoreflectance signal quality achieved with linear FM excitation are shown in Fig. 2.

APPARATUS

Fig. 3 shows a block diagram of the photothermoreflectance apparatus used in this work. The basic optical design was reported previously by Opsal et al [2] and is not discussed in detail here. In this work we have replaced the lock-in analyzer detection system reported previously with a sweep synthesizer and FFT analyzer (HP3562A dynamic waveform analyzer) for implementation of FM time delay spectrometry. The excitation bandwidth of the present system is 0-100 KHz and is limited by the bandwidth of the FFT analyzer. Detection of the reflectivity signal was achieved by means of a quad cell detector operating in the sum mode.

The thermal response of semi-infinite samples of quartz, stainless steel, aluminum and polyvinylidene difluoride (PVDF) were used to characterize the observed response of the apparatus. The quartz samples were surface deposited with a thin layer of gold to promote surface absorption. The PVDF film (28 μm) was surface aluminized so that optical radiation was absorbed within a few electromagnetic skin depths of the surface. The metallic samples were prepared by milling.

ANALYTICAL CHARACTERIZATION OF THERMAL SIGNALS

The experimental thermoreflectance response was compared to the theoretical semi-infinite thermal response profiles reported in Part I of this work. The finite size of the probe beam intercepting the area heated by the pump beam was further taken into account by integration of the theoretical semi-infinite

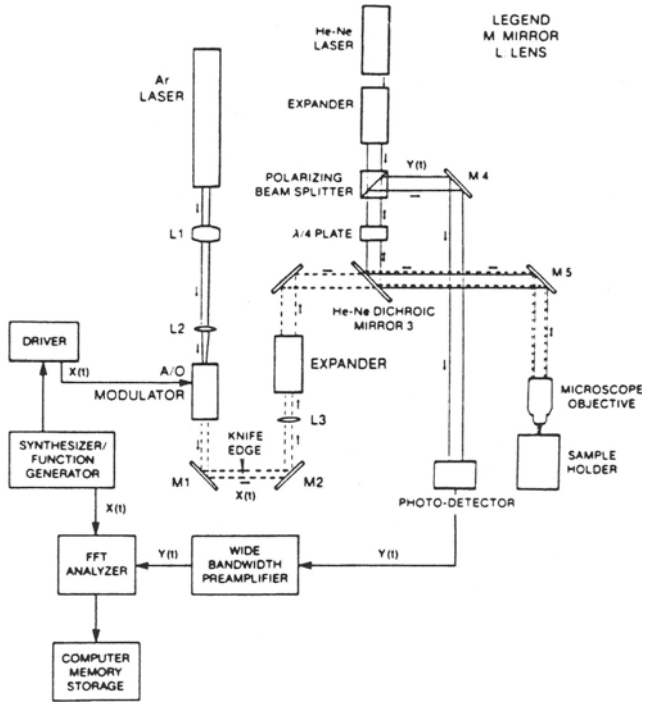

Fig. 3 Block diagram of impulse photothermoreflectance imager reported in this work.

Green's function over the transverse coordinates, assuming the probe beam was offset from the center of the pump beam by an amount r_b. The predicted temperature profile should then have the form:

$$h(t) = \frac{A_0\tau_0}{2(t+\tau_1)t^{1/2}} e^{-r_b^2/4\alpha(t+\tau_1)} \quad ; \tag{2}$$

$$\tau_0 = w_1^2/4\alpha \qquad \tau_1 = [w_0^2 + w_1^2]/4\alpha$$

where $h(t)$ is the photodetector signal, w_0 is the pump beam spot size, and w_1 is the probe beam spot size.

SIGNAL ANALYSIS AND MEASUREMENT PERFORMANCE

The first test of the validity of the FM Time delay measurement was a comparison of the frequency response data recovered using the wideband strategy with measurements made using steady state sinusoidal point-by-point excitation. As seen in Fig. 4, frequency swept measurements made over the full span of the analyzer at a sweep rate of 1.25×10^7 Hz/s (Fig. 4a) agreed well with slowly swept data (Fig. 4b). This test effectively eliminates response non-linearities which potentially arise in diffusive (i.e. thermal) systems at very high sweep rates. The frequency response profiles also indicate a band limitation imposed by the analyzer itself, since there is a significant component of sample response at 100 KHz. The effect of the abrupt truncation at 100 KHz is to introduce a contribution of early time "ripple" in the impulse response due to the well known leakage or "Gibb's phenomenon". Because the analyzer imposes its own band limit on the response signals, the width or duration of $R_{xx}(\tau)$ is not negligible compared with $R_{yy}(\tau)$, and the approximation of the input autocorrelation function to a Dirac Delta function is not strictly valid. The frequency domain division implied by Eq. (1b) is, however, sufficient to correct the recovered frequency response for any non-uniformities in the input power spectrum within the analyzer span as clearly evidenced by the results of Fig. 4.

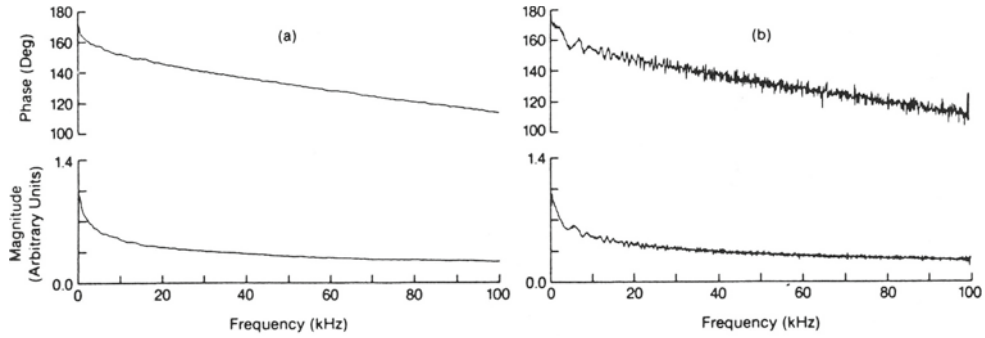

Fig. 4 Frequency response profiles recorded for semi-infinite quartz: (a) point-by-point slow sine sweep from 0 to 100 kHz, with 50 ms integration time per point; (b) FM linear sweep response from 0 to 100 kHz with S = 1.25×10^7 Hz/s and N = 1,000 averages.

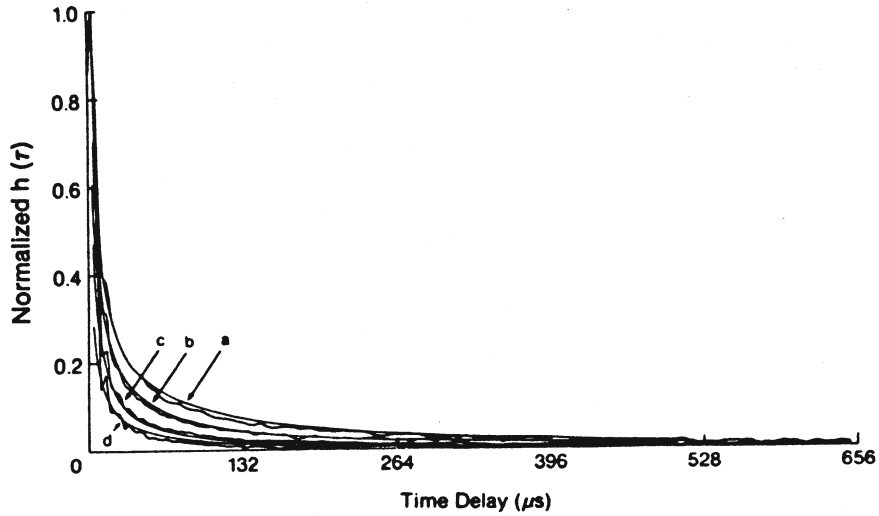

Fig. 5 Normalized impulse response profiles recorded for semi-infinite quartz with various values of w_0 and w_1. Theory vs. experiment. Upper curve: (a) w_0 = 14 μm; w_1 = 12 μm; (b) w_0 = 10 μm; w_1 = 8 μm; (c) w_0 = 8 μm; w_1 = 2 μm; (d) w_0 = 2 μm; w_1 = 6 μm. These results were obtained with linear FM sweep excitation and a frequency span of 0 to 100 kHz. Theoretical curves assume α_2 = 5×10^{-7} m^2/s for quartz. Each trace is the result of 1,000 averages. Beam diameters were estimated independently.

Experimentally recovered impulse response profiles for different combinations of pump and probe beam spot sizes are compared with the theoretical results of Eq. (2) in Fig. 5. These data, recovered for a semi-infinite quartz sample, show a good fit to the theory for data points recovered at time delays greater than 10 microseconds past excitation. In the present experimental situation the radial offset between beams was clearly negligible. The effect of increasing the pump beam spot size on the recovered response is to produce a gradual transition from a three dimensional heat conduction process to a one dimensional process as discussed in Part I of this work. If the probe beam radius is expanded while the pump beam spot size is kept small, the effective aperture for integration of the reflectivity change is increased. An increasing contribution of radial heat conduction is weighted and integrated by the probe beam, causing a broadening of the observed impulse response profile. Accordingly, as w_1 approaches an infinite value, the observed impulse response approaches the form expected for a one dimensional heat conduction process.

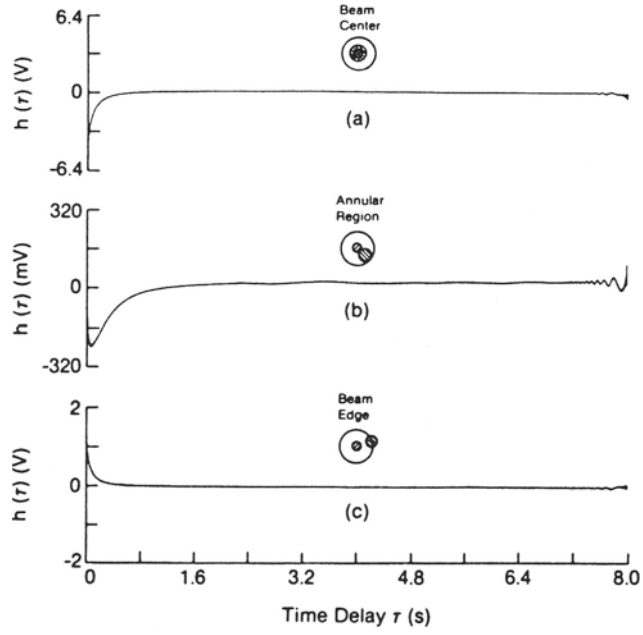

Fig. 6 Effect of thermal lensing on recovered impulse response. (a) response recovered with center of annular pattern sampled; (b) response recovered with rim of annular pattern sampled; (c) response recovered with beam edge sampled.

Additional complications of the thermoreflectance signal arise when the pump and probe beams are radially offset from each other. For the metallic and crystalline samples studied in this work, the errors lie within the frequency span of the analyzer.

COMPETITIVE PHOTOTHERMAL EFFECTS

Two important phenomena may complicate the thermoreflectance measurement. These effects consist of (a) thermal lensing in the gas layer due to heat conduction from the irradiated surface and (b) modulated thermoelastic deformations. Both effects have been investigated in detail by Opsal et al [2]. The thermal lens effect could be readily observed in these experiments by the visual monitoring of an annular interference pattern that formed in the detector plane when the heating beam was blocked and unblocked. The observed annular interference pattern may be explained through the refraction of light rays by a negative lens adjacent to the surface of the heated sample. The lens element in this case is smaller then the probe beam and is situated just past the probe beam waist so that the rays in the central section diverge. The focussing of a central section of the probe beam is observed if the probe beam waist is translated to a position behind the diverging lens element. The effect of thermal lensing on the recovered impulse response was examined by scanning an iris across the interference pattern observed in the detector plane (Fig. 6) (in this case due to thermal defocussing). Near the beam center, an initial negative transition in intensity is observed due to refraction by the lens element; the intensity recovers to its initial value as the refractive index gradient in the gas layer collapses. At the rim of the annulus, the initial effect is an interference of the refracted central section of the beam with an outer section which is weakly affected by the lens element.

It is clear that the signals shown in Fig. 6 although appearing on long timescales, produce an important spatial redistribution of the probe beam intensity, which varies significantly with the geometry of the pump and probe beams. The previous work of Opsal et al [2] clearly demonstrated the interference of gas phase thermal lensing in photothermoelastic effect measurements at frequencies approaching 1 MHz. It is

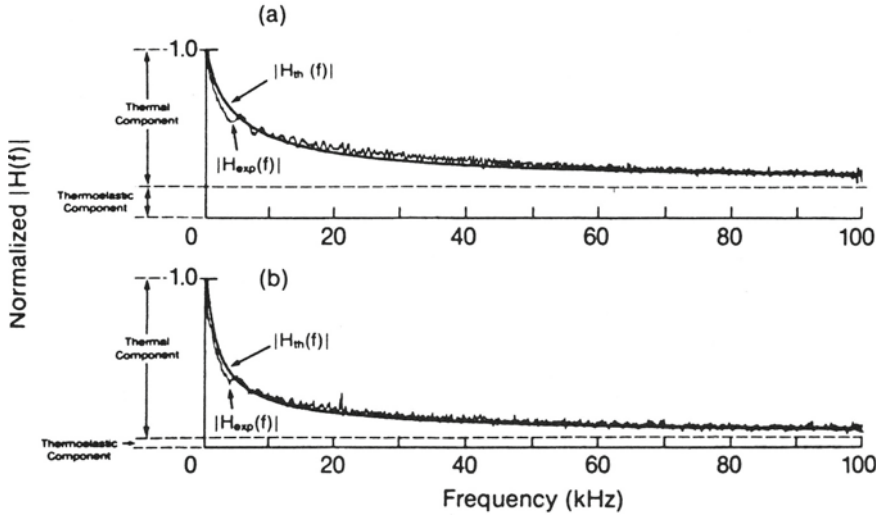

Fig. 7 Experimental transfer function, $H_{exp}(f)$, for semi-infinite quartz, and theoretical fit to magnitude response. The latter involves a purely thermal response component and a constant baseline. (a) $w_0 = 2\ \mu m$; $w_1 = 7\ \mu m$; n = 500 averages; (b) $w_0 = 14\ \mu m$; $w_1 = 12\ \mu m$; n = 1,000 averages. $\alpha_2 = 5\times10^{-5}\ m^2/s$.

worthy of mention that thermal lensing and in particular, thermally induced refraction effects may contribute significant errors in measurements where the reflectivity signal is weak, and where there is partial blockage of the analysis beam ahead of the detector plane.

In addition, the absorption of a highly focussed beam of radiation at the sample surface gives rise to thermoelastic deformations. These phenomena were studied in detail in past work [2], and, by means of beam deflection measurements were shown to possess very wide bandwidths. The deflection measurement is readily measured using a quad cell detector operating in the difference mode in which movements of the beam across the detector face are readily detected by means of the difference in response of two of the cell quadrants. The sum mode configuration adopted in the present work was initially expected to separate thermoelastic from thermoreflectance signals. However, a detailed analysis of the frequency and impulse response profiles studied indicated a deviation from the thermoreflectance theory which was immediately assignable to a "flatband" contribution of extraneous signal in the frequency domain. The flat response agrees well with the frequency response (magnitude) observed for the thermoelastic effects in this frequency range [2,7]. It was possible to resolve this flatband contribution by separating pump and probe beams with $r_b > w_1$ and recording the sample response. The frequency response (magnitude) observed with the beams separated was, in fact, flat within the analyzer bandwidth as expected for a thermoelastic interference.

REFERENCES

1. A. Rosencwaig, J. Opsal, W.L. Smith, and D.L. Willenborg, Appl. Phys. Lett. **46**, 1013 (1985).
2. J. Opsal, A. Rosencwaig, and D.L. Willenborg, Appl.Opt. **22**, 3169 (1983).
3. C.A. Paddock and G.L. Eesley, J. Appl. Phys. **60**, 285 (1986).
4. A. Mandelis, I.E.E.E. Trans. U.F.F.C., **UFFC-33**, 590 (1986).
5. R.C. Heyser, J. Audio Eng. Soc. **15**, 370 (1967).
6. J.S. Bendat and A.G. Piersol, *Engineering Applications of Correlation and Spectral Analysis*, (Wiley, New York, 1980).
7. A. Mandelis, A. Williams, and E. Siu, J. Appl. Phys. **63**, 92 (1988).

SINGLE BEAM INTERFEROMETRY OF A THERMAL BUMP: I -EXPERIMENT

P.K. Kuo and M. Munidasa

Department of Physics
Wayne State University
Detroit, MI 48202

INTRODUCTION

We present a sensitive interferometric technique which simultaneously measures the optical, elastic and thermal parameters of solids. We obtain the optical reflectivity change and the displacement due to thermal expansion (thermal bump) produced by an intensity modulated and focused laser beam.

In this scheme a probe beam larger than the size of the thermal bump is reflected from the sample surface. Earlier works [1] have used a probe beam smaller than the size of the thermal bump. The information is contained in the distortion of the reflected wave-front, caused by the thermal bump. This information about the material properties is obtained by measuring the interference pattern produced by the superposition of the distorted ac wave-front from the bump and the reflected undistorted dc wave-front from the surrounding surface (Figure 1). Interference patterns of this type has been observed before [2] in the reflected laser beam from a liquid surface. The interference pattern is measured by scanning a photo-detector across the reflected probe beam. Since only a single beam is used, noise from mechanical vibrations and fluctuations in air currents are greatly reduced. The signal is detected synchronously with the modulation of the thermal bump, using a lock-in amplifier. Experimental data are fitted to a phenomenological theory using a multi-parameter least-squares fit routine. Optical and thermal parameters are deduced from these fits.

EXPERIMENTAL METHOD

Figure 2 depicts the experimental arrangement used. The heating beam is obtained from the 4880 Å line of an Argon ion laser, intensity-modulated by means of an acousto-optic modulator, and subsequently focused to a ~10 μm spot on the sample surface. The average incident power is about 40 mW. The 6328 Å beam from a 3 mW He-Ne laser is used as the probe beam. This beam is not focused, and has a spot diameter of about 800 μm at the sample. The heating beam spot can be laterally displaced with respect to the center of the probe beam spot by moving the focusing lens. The probe beam reflected from the sample surface is detected by a photodiode with a slit (width of ~50 μm) in front of it. The photodiode (without the slit) is large enough to capture the entire probe beam. The detector/slit assembly is scanned across the beam using a stepping-motor-driven scanning stage to record the interference pattern. The signal is synchronously detected by a lock-in amplifier. The data are collected by a micro-computer which also controls the stepping motor.

A detailed knowledge of the probe beam's characteristics is essential in the quantitative analysis of the data. The position and magnitude of the Gaussian beam waist are separately determined by measuring the beam profile at several distances on the same setup with a chopped probe beam.

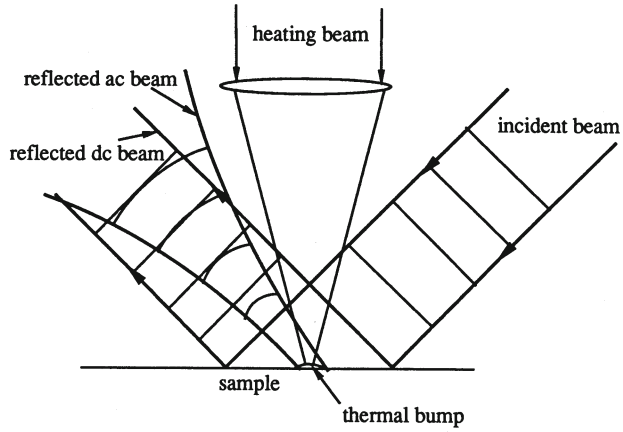

Fig. 1. Wave front figure of the incident and the reflected probe beam.

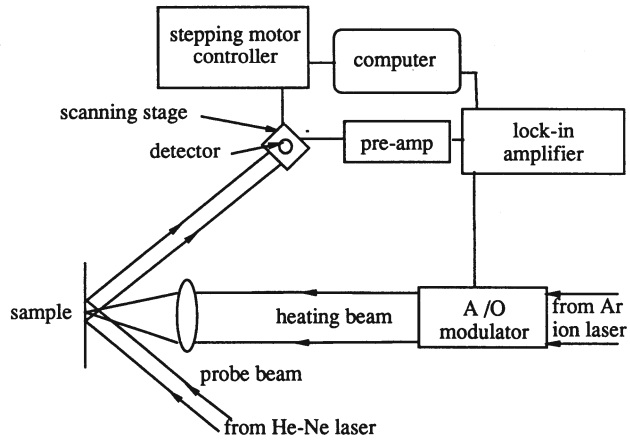

Fig. 2. Experimental arrangement.

Using our interferometer on a silicon wafer we are at present able to get a usable signal (with a 1-second time constant) with a heating beam power as low as 0.1 mW (Figure 3). This corresponds to a bump height of ~ 10^{-3} Å at 1 kHz. We have not yet achieved sensitivities reported by other interferometric techniques.[3-5] Those techniques, however, use much more elaborate experimental arrangements than that described here.

PHENOMENOLOGICAL THEORY

The interference between spherical (from the bump) and a planar wavefronts (from the surrounding surface) gives rise to the traditional pattern of Newton's rings. Due to the small size of both the thermal bump and the probe beam, only two or three of the rings are visible at an experimentally convenient distance. To obtain quantitative information from such an interference pattern, the traditional fringe counting method would be too imprecise. Ideally one would want to do a least-square fit of the measured data to a theoretical calculation of the fringe pattern based on the detailed shape and time variation of the thermal bump. Such a calculation from first principles is being undertaken by Favro and Munidasa [6]. In this report we present a more heuristic approach to the analysis of acquired data.

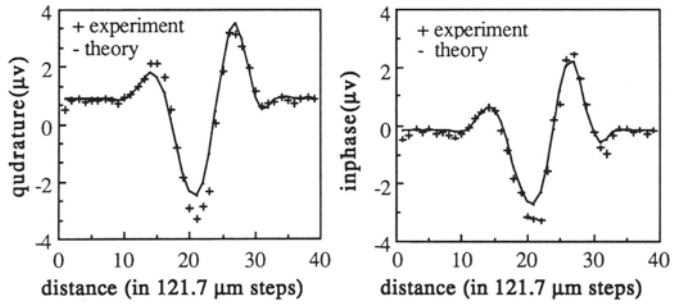

Fig. 3. Experimental data and theoretical fit of inphase and qudrature signal for a Si wafe with a heating beam power of 0.1 mW and a modulation frequency of 1 kHz. Bump height calculated from the fit is 3 x 10^{-3} Å.

We make a simplifying assumption that the height of the thermal bump has a Gaussian shape and that the entire bump has a spatially uniform phase which follows the modulated heating beam. Accordingly we express this height as

$$h\,(x,y,t) \;=\; \delta h \cos\,(\Omega t + \theta_h)\, \exp\,[-(x^2+y^2)/r_b^2] \quad , \tag{1}$$

where δh is the amplitude, θ_h is the phase and r_b is the Gaussian radius of the bump. The (angular) frequency of the heating modulation is Ω. These assumptions are somewhat arbitrary for the general situation, but they are quite reasonable in cases for which the thermal diffusion length of the sample is much less than the radius of the heating beam. In these cases the thermal bump barely extends beyond the heating beam profile and follows the phase of the latter. This situation can be attained experimentally by using a high modulation frequency, or a large heating beam or a combination of both. If the phase distorsion introduced by a Gaussian surface is small, the resulting reflected beam can still be handled by Gaussian optics. This assumption obviates the need of a time-consuming diffraction calculation from the sample surface to the detector and permits us to explore the essential physics of the situation.

We will be making use of the complex representation of the Gaussian beam in the form of a modified spherical wave propagating in the positive z direction:

$$E(x,y,z,t) = E_0 \frac{-iz_0}{z - z_1 - iz_0} \exp ik\left[z + \frac{x^2 + y^2}{2(z - z_1 - iz_0)}\right] \quad , \tag{2}$$

where E_0 is the amplitude of the electric field, k is the optical wave number, the real constant z_0 defines the waist size w_0 (at $z = z_1$) through

$$z_0 = w_0^2 k/2 \quad . \tag{3}$$

Since this form can be derived from the following exact solution to the wave equation

$$E(x,y,z,t) = E_0 e^{ik\rho}/\rho \quad , \tag{4}$$

where

$$\rho = \sqrt{x^2 + y^2 + (z - z_1 - iz_0)^2} \quad , \tag{5}$$

by making expansions appropriate in the Fresnel regime ($x,y << |z-z_1-iz_0|$), it correctly describes the propagating behavior of a Gaussian beam. That is, if a light beam is known to be Gaussian at one position of z (i.e., its radial intensity and phase distributions are Gaussian) then by matching it with the expression (2) the characteristics of this beam at any other position of z is known. This is the basic technique we have used to avoid a diffraction calculation. In this analysis two important effects will be treated. The first is the phase change introduced by the sinusoidally moving reflecting sample surface (assuming normal incidence). The second is the slight intensity change caused by the sinusoidally varying reflectivity of the surface which, in turn, is a result of the modulated heating. The amplitude reflection coefficient of the sample surface will be modeled as

$$R(x,y,t) = R_0 + \delta R \cos(\Omega t + \theta_R) \exp[-(x^2+y^2)/r_b^2] \quad , \tag{6}$$

where R_0 is the amplitude reflection coefficient of the unheated sample surface and θ_R is the phase of the temperature variation. We have implicitly assumed that the modulated temperature distribution has the same Gaussian radius as the thermal bump in the same spirit of the earlier assumption. We introduce these effects into the calculation by the following multiplicative factor to the amplitude of the optical wave

$$R(x-x_1,y,t) \exp[-2ik\, h(x-x_1,y,t)] \quad , \tag{7}$$

where we have placed the center of the thermal bump at $x=x_1$, $y=0$. Keeping in mind the fact that the maximum height of a typical thermal bump is much less than 1Å, the quantity in the exponent in (7) is always much than unity. The following approximation is therefore valid.

$$\exp[-2ik\, h(x-x_1,y,t)] = 1 - 2ik\, h(x-x_1,y,t) \quad . \tag{8}$$

When a detector with a narrow slit along the y-direction is scanned in the x-direction, the received signal is the intensity of the reflected beam integrated along y-direction. In the integrated result there are dc terms, terms with frequency Ω and terms with frequency 2Ω. Only the terms with frequency Ω will be detected by the lock-in amplifier. They represent essentially the interference between the dc and the ac components of the beam and are linear in the small quantities δh and δR.

The final expression for the lock-in detected interference signal is quite lengthy and cumbersome, but it can be summerized simply as

$$\exp(a + rx + px^2) \cos(b + tx + sx^2) \quad , \tag{9}$$

with

$$a + ib = \frac{1}{2} \ln \frac{2\pi}{ik} + \ln (I_0 z_0^2) + \ln \frac{z_1' - iz_0'}{z_1 - iz_0} + \ln \left[\frac{\delta R}{R_0} \cos \theta_R - 2ik\, \delta h \cos \theta_h \right]$$

$$- \frac{1}{2} \ln \left\{ \left[(z_1' - z_1) - i(z_0' + z_0) \right] (z_1 + d + iz_0) (z_1' + d - iz_0') \right\}$$

$$- i \frac{kx_1^2}{2} \frac{\left[(z_1' - z_1) - i(z_0' - z_0) \right] (z_1 + d - iz_0)}{(z_1' + d - iz_0')(z_1 - iz_0)^2} \quad , \tag{10}$$

$$r + it = ikx_1 \frac{\left[(z_1' - z_1) - i(z_0' - z_0) \right]}{(z_1' + d - iz_0')(z_1 - iz_0)} \quad , \quad \text{and} \tag{11}$$

$$p + is = - \frac{ik}{2} \frac{\left[(z_1' - z_1) - i(z_0' + z_0) \right]}{(z_1' + d - iz_0')(z_1 + d + iz_0)} \quad , \tag{12}$$

where I_0 is the reflected beam intensity ($=R_0^2 E_0^2$), x_1 is the offset between the centers of the probe and heating beams, and d is the sample to detector distance. The constants z_0 and z_1 are the beam parameters of the probe beam as defined in (2). The constants z_0' and z_1' are the corresponding parameters of the ac beam which results from the diffraction from the thermal bump, they are related to z_0 and z_1 through a lens-like equation

$$\frac{1}{z_1' - iz_0'} - \frac{1}{z_1 - iz_0} = \frac{2i}{kr_b^2} \quad . \tag{13}$$

The constants a, b, r, t, p, and s can be obtained from a least-square fit to the measured dc beam intensity profile and the ac interference pattern. The unknown quantities δR, δh and r_b also emerge from the least-square fit. Note that the first two appear together only in the combination

$$\frac{\delta R}{R_0} \cos \theta_R - 2ik\, \delta h \cos \theta_h \quad . \tag{14}$$

Since θ_R and θ_h are measured relative to the phase setting of the lock-in amplifier, the quadrature signal of a vector lock-in amplifier gives the same result except that the cosine functions in Eq.(14) are replaced by sine functions. This permits both $\delta R/R_0$ and δh to be determined independently.

RESULTS

In order to verify the general correctness of the above phenomenological theory, we made several scans changing only the value of x_1. Figure 4 shows the result of such scans compared with the curves calculated from Eq. (9) with values of parameters determined by a least-square fit. The fit is not as good towards the shoulders of the beam. This is attributable to the same observed deviation of the profile of the dc beam from a perfect Gaussian distribution.

We have applied this interferometric technique to a silicon wafer which has a doped (with boron, to 10^{16} cm^{-2}) region. Figure 5 shows the resulting bump heights from both doped and undoped regions as a function of the modulation frequency.

CONCLUSIONS

We have reported a novel single beam interferometric technique which has quite good sensitivity. The main advantage of this method is its simplicity in experimental arrangement. A single unfocused laser beam is used and there is not a single optical component between the laser and the detector except the sample surface. It must be kept in mind, however, this method is

limited to samples whose surfaces are specular reflectors. Pending more theoretical development, this method should be very suitable to thin film materials. Because of the thermoelastic process involved in this kind of interferometry, it should be especially good in determining adhesion property of thin films to their substrates.

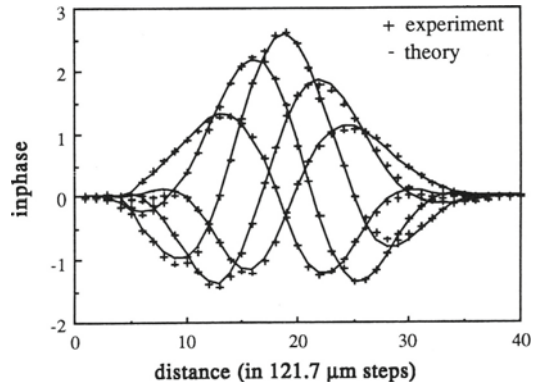

Fig. 4. Experimental data and the theoretical fit of the inphase signal, for five different heating beam positions within the probe beam.

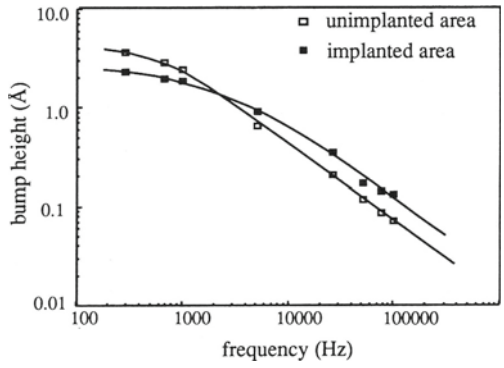

Fig. 5. Plot of bump height vs.frequency of the unimplanted region and a implanted region (50 kev B^+, 10^{16} ions/cm^2) of a p-type Si wafer.

ACKNOWLEDGEMENT

This work was sponsored by the Institute for Manufacturing Research, Wayne State University, Detroit, Michigan.

REFERENCES

1. A. Rosencwaig, J. Opsal, W.L. Smith, and D.L. Willenborg, J. Appl. Phys. **59**, 15 (1986).
2. J. Hartikainen, J. Jaarinen, and M. Luukkala, Can. J. Phys. **64**, 1341 (1986).
3. D. Royer and E. Dieulesaint, Appl. Phys. Lett., **49**, 1056, (1986).
4. H.K. Wickramasinghe, Y. Martin, D.A.H. Spear, E.A. Ash, J.Physique.Coll. C6, **44**, 191 (1983).
5. M.A. Olmstead, N.M. Amer, S.E. Kohan, D. Fournier, A.C. Boccara, Appl. Phys. A, **32**, 141 (1983).
6. L.D. Favro and M. Munidasa, in Reviwe of Progress in Quantitative NDE, Ed. D.O. Thompson and D.E. Chimenti, Vol 8 (to be published).